Thin Solid Films 582 (2015) 2–6

Contents lists available at ScienceDirect

Thin Solid Films

journal homepage: www.elsevier.com/locate/tsf

Controlled bandgap $CuIn_{1-x}Ga_x(S_{0.1}Se_{0.9})_2$ ($0.10 \leq x \leq 0.72$) solar cells from electrodeposited precursors

João C. Malaquias [a,*], Dominik M. Berg [b], Jan Sendler [a], Marc Steichen [a], Nathalie Valle [c], Phillip J. Dale [a]

[a] University of Luxembourg, Physics and Materials Science Research Unit, 41, rue du Brill, L-4422 Belvaux, Luxembourg
[b] University of Delaware, Institute of Energy Conversion, 451 Wyoming Rd., Newark, DE 19716, USA
[c] Centre de Recherche Public Gabriel Lippmann, 41, rue du Brill, L-4422 Belvaux, Luxembourg

ARTICLE INFO

Available online 25 October 2014

Keywords:
Electrodeposition
CIGS
Gallium segregation
Annealing
Photovoltaics
Ionic liquids
Deep eutectic solvent

ABSTRACT

Electrodeposition and post-annealing is a potentially low-cost industrial growth route for $Cu(In,Ga)(S,Se)_2$ solar cells. Nevertheless, this process is limited by the difficulty to introduce gallium in the precursor and by the segregation of gallium during the annealing step. Previously, we countered the former problem by co-electrodepositing In and Ga from a Deep Eutectic Solvent, accurately controlling the Ga/(Ga + In) (referred to as Ga/III) ratio of the precursor. In order to avoid segregation we employed a three-step annealing procedure, introducing a limited quantity of sulphur on the surface of the absorber. In this work, absorbers and solar cells originating from electrodeposited precursors with $0.10 \leq Ga/III \leq 0.72$ are characterised. X-ray diffraction results show that the $Cu(In,Ga)Se_2$ 112 peak shifts to higher angles with increasing Ga content, in agreement with the expected composition values. Additionally, these results show identical incorporation of sulphur in all samples. Photoluminescence, external quantum efficiency, and current–voltage measurements corroborate the X-ray diffraction results. Controlled incorporation of Ga, over a large Ga/III range, is achieved for electrodeposited and post-annealed $Cu(In,Ga)(S,Se)_2$ absorbers. A maximum solar cell efficiency of 9.8% was obtained.

1. Introduction

Solar cells based on $Cu(In,Ga)(S,Se)_2$ (CIGSSe) are one of the best performing thin film technologies, achieving efficiencies of 21% in the laboratory environment [1]. However, these devices are produced by vacuum methods, which prevent cost reduction at industrial level. Electrodeposition and post-annealing (EDA) is a low-cost growth method which can replace these evaporation methods. This process is hindered by two factors: i) The electrodeposition of Ga from aqueous electrolytes is hindered by the occurrence of the competing Hydrogen Evolution Reaction during deposition, reducing the process efficiency [2] and leading to the incorporation of oxides and hydroxides; and ii) Ga commonly segregates to the back of the absorber layer during annealing, forming a $CuInSe_2/CuGaSe_2$ system. In our previous work, we reported on the efficient electrodeposition of Cu(In,Ga) metal precursors with controlled composition ($0 \leq Ga/(Ga + In) \leq 1$), by using a non-toxic and inexpensive deep eutectic solvent as electrolyte [3–5]. In the following discussion, the Ga/(Ga + In) ratio will be referred to as Ga/III, for simplicity.

Gallium segregation typically occurs in two-step processes such as EDA [2] and sputtering and annealing [6], severely hindering solar cell performance due to the open circuit voltage (V_{oc}) limitation.

Recently Kim et al. reported a three-step annealing process, for co-sputtered metal precursors, avoiding Ga segregation and delivering absorber layers with nearly flat Ga profile in the bulk and a slight Ga depletion near the surface [7,8]. In this work, we apply the annealing method developed by Kim and co-workers to electrodeposited metal precursors. We show that this process is adequate to treat our precursors and demonstrate that CIGSSe, with varying Ga content, can be grown from electrodeposited precursors. To this end, semiconductor properties and solar cell electrical parameters were studied as a function of the Ga/III ratio in CIGSSe absorbers, since these consistently change with different Ga content. In this manuscript the acronym for the chalcopyrite compounds will end in “Se” for pure selenide materials (e.g. CISe, CGSe) and in “S” for pure sulphide materials (e.g. CIS, CGS).

2. Experimental

The Cu(In,Ga) metal precursors used in this study were deposited by electrodeposition from a deep eutectic solvent. Extensive details can be found in Ref. [4]. Briefly, a copper layer was electrodeposited on a soda lime glass (SLG) substrate with a sputtered Mo coating, followed by indium and gallium coelectrodeposition. These metal precursors were then annealed at the Institute of Energy Conversion of the University of Delaware (IEC) with the process described in Ref. [8]. In short, this process comprises three different steps. The first step consists of annealing the precursor in the presence of H_2Se, followed by a second thermal

* Corresponding author. Tel.: +352 466644-5860; fax: +352 466644 36156.
E-mail address: joao.malaquias@uni.lu (J.C. Malaquias).

http://dx.doi.org/10.1016/j.tsf.2014.10.068
0040-6090/

treatment solely in the presence of inert Ar gas. In the third and last step the films are annealed in the presence of H_2S, introducing a limited quantity of sulphur into the surface of the absorber ($S/(S + Se) \approx 0.1$) [8]. The composition and thickness of the absorbers were measured by X-ray fluorescence (XRF) in an X-Strata by Oxford Instruments. The crystal structure of the films was characterised by X-ray diffraction (XRD) using a Brüker D8 Discovery diffractometer. The wavelength of the incident radiation was $\lambda = 1.5418$ Å ($Cu\ K_\alpha$). Room temperature photoluminescence (PL) measurements were carried out by exciting the absorbers with the Ar ion laser 514.5 nm line. In order to collect the PL photons, both InGaAs and Si detector arrays were used. Solar cells were finished in the configuration SLG/Mo/CIGSSe/CdS/i-ZnO/ITO/Ni–Al. Details on the deposition of the last four layers of the solar cell can be found in Ref. [8]. Three individual solar cells, each with a surface area of 0.47 cm^2, were fabricated on each absorber. Within the same absorber, the device efficiency varied, on average, by 59%, here we only consider the best performing solar cell from each absorber. External quantum efficiency (EQE) measurements were performed on the solar cells as well as current density–voltage (j–V) measurements under simulated AM 1.5 illumination at 25 °C and with an intensity of 1000 $W \cdot m^{-2}$. The j–V measurements were performed over the full area of the device and the EQE measurement area was a spot with a surface area of 4 mm^2. All solar cell parameters were extracted from the illuminated j–V curves, except for the parallel conductance which was extracted from the dark j–V curve, using the method described by Hegedus et al. in reference [9]. Secondary ion mass spectrometry (SIMS) measurements were performed in a CAMECA SC-Ultra instrument. The in-depth composition profiles were obtained via bombardment with $^{133}Cs^+$ ions, accelerated with 4.5 kV. In order to minimise matrix effects, gallium and sulphur were measured as $GaCs^+$ and SCs_2^+ clusters, respectively. The area of analysis had a diameter of 33 μm. The depth axis was estimated using the value of the absorber layer thickness obtained by XRF.

Table 1 presents the XRF results on the Cu/(Ga + In) (Cu/III) and the Ga/III ratios for the different absorbers, which are named in text by GA followed by their Ga/III ratio determined by XRF. From Table 1 one can observe that the absorbers are Cu-poor, in line with the expected value of 0.85, except for sample GA048 which is near stoichiometric. All absorbers present a thickness around 1300 nm and were subjected to the same annealing process, only absorber GA048 was formed in a different run under the same conditions.

3. Results and discussion

First we characterise absorbers with different Ga contents and the corresponding solar cells. The characterisation focuses on the optoelectronic properties of the semiconductor and on the electrical performance of the solar cells. These results demonstrate that the employed annealing is efficient in delivering CIGSSe with controlled bandgap and avoid CISe/CGSe segregation. Then the most efficient solar cell is discussed.

Fig. 1a depicts the normalised intensity XRD diffractograms of CIGSSe absorbers with different Ga content measured in a θ–2θ configuration around the chalcopyrite 112 plane.

The diffractograms show that all peaks are located between the pure CISe and CGSe 112 maxima (JCPDS card-files 40-1487 and 31-0456, respectively) and shift to higher angles with higher Ga/III ratio, as expected [10]. Less intense peaks are detected for $2\theta \geq 27.9°$, corresponding to CIGS phases. The normalised intensity of the CIGS peaks is below 0.05 and similar in all diffractograms, suggesting limited and identical sulphur incorporation in all absorbers. Additionally, Kim and co-workers observed that sulphur was present solely on the surface of the absorber (around 50–60 nm), which is in accordance with the SIMS results in Fig. 1b [8]. These observations indicate that the shift of the CIGSe 112 peak is not related to sulphur incorporation, but rather gallium.

The full width at half maximum (FWHM) of the peak was calculated using the equation in Ref. [11] and varied between 0.19° and 0.23°. This result is similar to what was obtained for evaporated CIGSe layers with different Ga contents. In their work, the authors obtained $0.15° \leq FWHM \leq 0.19°$ for the 112 peak [12].

The near identical FWHM and the fact that the 112 peaks have a symmetric shape, suggest that in the bulk of the absorber there is no significant Ga gradient. Although XRD analysis shows no signs of Ga segregation, SIMS analysis reveals Ga accumulation at the back of absorber GA072, suggesting its presence in a Ga-rich CIGSe phase (cf. Fig. 1b).

The Ga/III ratio of the absorbers was derived from both the CIGS and the CIGSe 112 peak positions. This derivation process involves three steps: in the first, the lattice parameters, with varying gallium content, are calculated using the models in Ref. [13] for CIGSe and Ref. [14] for CGS, being followed by the determination of the respective 112 interplanar distances, using the equation for the tetragonal crystal lattice system. In the third step, the reference 112 Bragg angles are calculated using Bragg's Law and the calculated interplanar distances. With these calculations, a range of Bragg angles, which are related to the gallium content, are obtained and thus the Ga/III ratio can be derived from the peak position. The values obtained are present in Table 1. The uncertainty associated to these values derives from the position of the Mo 110 peak, which was constantly shifted by +0.03° from its reference position (JCPDS card-file 42-1120), giving rise to a deviation of 0.03 on the Ga/III ratio.

The Ga/III values obtained from the CIGSe peaks are systematically lower but in good agreement with the ones obtained by XRF. Regarding the CIGS 112 maxima, the derived Ga/III values are coincident with those determined by XRF. This result suggests slightly higher gallium content at the surface. Additionally, the fact that the Ga/III values obtained by XRF and from the two sets of XRD peaks are in good agreement, indicates that there is little intermixing between the selenide and sulphur phases.

As previously referred, from the XRD data it is concluded that, at the surface, the Ga content is higher. This observation is in agreement with the SIMS profile in Fig. 1b for all absorbers. However, the same plot shows that at the CIGSe/CIGS interface there is Ga depletion on the CIGSe side. It is known for SIMS measurements that a change in the matrix, i.e. a transition from CIGSe to CIGS, can change the measured intensity for the same element, in this case Ga. However, the existence of this v-shaped Ga gradient (schematised in Fig. 1c) appears to be real, as adequately explained by the following PL results.

Table 1
Absorber composition obtained from different characterisation methods and solar cell parameters as obtained from j–V analysis. The figures between brackets are the errors associated to the values.

Absorber	Cu/III (±0.02)	Ga/III as obtained from:					η/%	FF/%	V_{oc}/mV	J_{sc}/mA·cm^{-2}
		XRF (±0.02)	XRD (±0.03) CIGSe	XRD (±0.03) CIGS	PL (±0.01)	EQE (±0.05)				
GA048	0.98	0.48	–	–	–	–	9.8	54	676	27.1
GA013	0.93	0.13	0.08	0.09	0.04	0.00	7.3	48	467	32.4
GA035	0.86	0.35	0.32	0.34	0.20	0.22	6.1	42	551	26.3
GA057	0.85	0.57	0.53	0.57	0.30	0.46	5.4	38	635	22.6
GA072	0.83	0.72	0.65	0.73	0.35	0.60	4.8	39	672	18.6

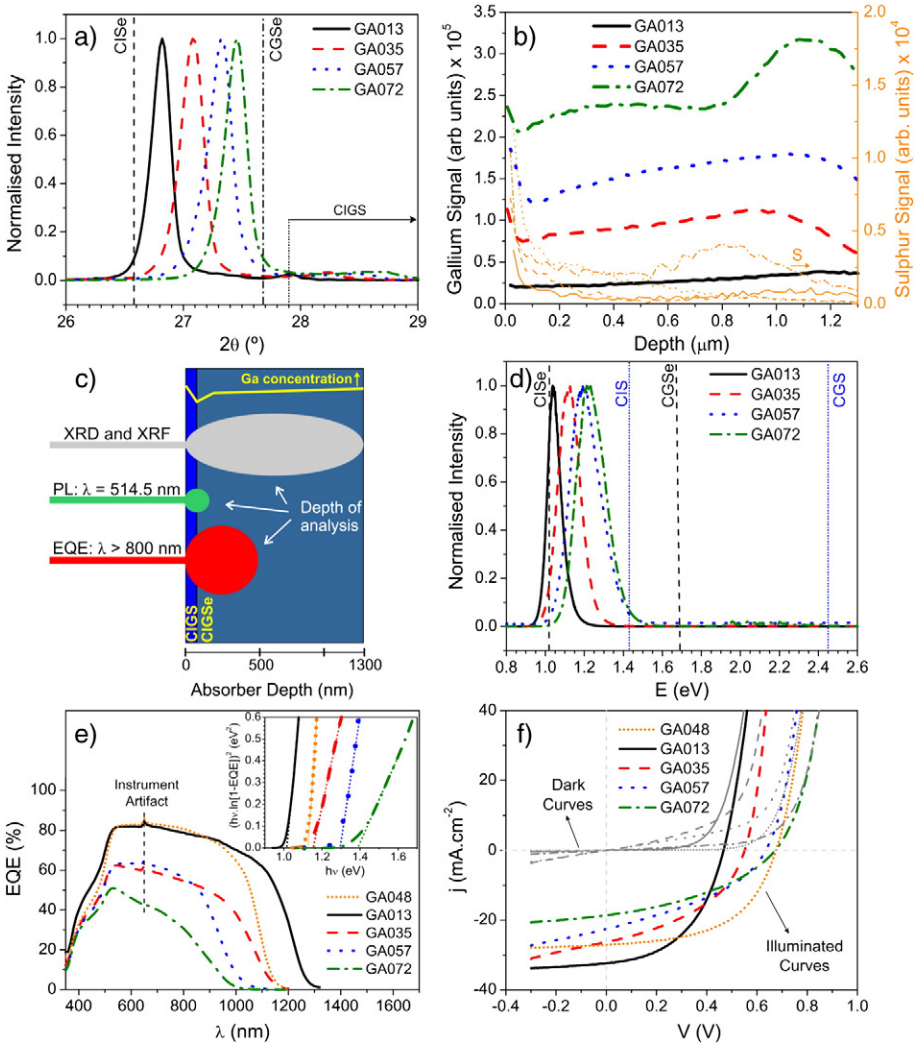

Fig. 1. a) Normalised XRD diffractograms of CIGSSe absorbers. SIMS gallium (thicker lines) and sulphur (thinner lines in orange) profiles of CIGSSe absorbers are depicted in b). The naming of the sulphur profiles follows the same line style as that of the gallium profiles. The depth of analysis of each characterisation method is shown in c). The same figure schematises the Ga profile in the absorber. It is intended to highlight the V-shape profile at the CIGSe/CIGS interface. The normalised room temperature PL spectra are depicted in d). The external quantum efficiency measurements of the matching solar cells are depicted in e) and f) shows their dark (in grey) and illuminated j–V curves. The naming of the dark j–V curves follows the same line style as that of the illuminated curves. The inset in plot e) depicts the bandgap determination from the EQE data.

Fig. 1d depicts the room temperature PL spectra of the absorbers. PL peaks corresponding to band-to-band transitions are observed and shift to higher energies with higher Ga content, as expected [10]. Although it was expected to observe two sets of peaks, one set for CIGSe and one set for CIGS, no CIGS PL peaks are detected. This result suggests that the CIGS layer on the surface is highly defective and dominated by non-radiative recombination. Another possibility is that charge carriers generated at the CIGS layer diffuse to the CIGSe bulk, driven by the difference in the energy bands, due to the different bandgaps. Thus, the recombination of these charge carriers would contribute to the CIGSe PL signal. It is observable that the CIGSe peaks become broader with increasing Ga/III ratio, indicating that for the same interaction volume, a wider range of bandgaps, i.e. Ga/III ratios, are detected. Such a finding is related to the Ga depletion found at the Se side of the CIGSe/CIGS interface (Fig. 1b and 1c) and to the fact that the PL signal comes from this region, since the laser penetration depth (depicted in Fig. 1c) is around 100 nm [15]. Additionally, this observation indicates the Ga gradient at this interface is increasingly steeper with the Ga content, since there is a wider range of bandgaps for the same probed volume. SIMS analysis confirms this trend (cf. Fig. 1b). From the peak position, the Ga/III value is calculated using the equation present in Ref. [16], which relates the bandgap to the gallium content. The error of the PL is approximately 10 meV due to the difficulty in determining the peak maximum, implying an uncertainty on the Ga/III ratio of 0.01. The calculated Ga/III values are in Table 1. These values are lower than the ones determined by XRD and XRF. The difference increases with the Ga/III ratio as a consequence of the steeper Ga gradient at the CIGSe/CIGS interface. Therefore, the bandgap obtained from these measurements is not representative of the bulk of the absorber. Nonetheless, since the PL signal is originating from pure selenide material, the variation of the bandgap is due to different Ga content. Additionally, the PL data in combination with the XRD results, confirms the v-shaped gradient at the CIGSe/CIGS interface, as depicted in Fig. 1b.

Fig. 1e depicts the EQE of the corresponding solar cells. In general, the magnitude of the EQE across the entire wavelength range decreases as the Ga/III ratio increases. Cell GA035 is an exception to this trend, but by a marginal difference. Such observation suggests that the performance of the solar cell becomes worse with higher Ga content and is in line with previous findings [17]. Nonetheless, the magnitude of the EQE curve for cell GA035 is much lower than expected since its Ga content is near the empirical ideal value, suggesting that other factors limit the performance. The inset in Fig. 1e shows the bandgap determination from the EQE measurements. The bandgap increases with the Ga/III ratio as expected and in line with the PL results. The Ga/III ratio was

extrapolated from the bandgap, however its error is higher than the PL-calculated value, since it is based on an indirect measurement of the bandgap and because it can be influenced by a poor charge carrier collection. For GA013 the Ga/III ratio as deduced from the bandgap is zero, in contrast with the values from the other methods, but still compatible to the one obtained by PL. For device GA035, a Ga/III = 0.22 is calculated from the EQE, which is in line with the value from PL, but lower than the ones obtained by XRD and XRF. For the remaining devices, the Ga/III ratio is higher than the ones obtained from PL and increasingly closer to the values given by the XRD. These observations indicate that there is a slight gallium gradient in the bulk of the absorber as well (Fig. 1c). The bandgap is obtained by evaluating the EQE for $\lambda > 800$ nm and photons of these wavelengths are absorbed until 500 nm depth (Fig. 1c) [15]. Hence, for an increasing gallium content, the closer the composition is to the value derived from the XRD, the narrower the graded region in the bulk is. This observation is supported by SIMS analysis, despite the differences being small and film GA072 displaying Ga accumulation at the back (cf. Fig. 1b). Moreover, the Ga profile is flatter with higher Ga/III, even for film GA072, if the region with Ga accumulation at the back is disregarded.

This observation is in good agreement with what was discussed by Marudachalam and co-workers, who reported that the homogenisation of the Ga profile in CIGSe with lower Ga content requires higher temperatures or longer annealing times [18].

Fig. 1f presents the j–V curves of the corresponding solar cells. The electrical parameters for these devices are shown in Table 1.

The efficiencies of the devices decrease with increasing Ga/III, in line with the expectations from the EQE results. The open circuit voltage (V_{oc}) increases with higher Ga content while short circuit current density (J_{sc}) decreases. Both trends are in line with the theoretical expectations and are linked to the bandgap increase with higher Ga content [19]. The J_{sc} values from the j–V curves for devices GA035, GA057 and GA072 are 16–45% higher than the ones obtained by integrating the product of the EQE by the AM1.5 photon flux. This observation suggests that the absorbers are not laterally uniform because the J_{sc} obtained from j–V is normally only up to 5% lower than the J_{sc} obtained from EQE due to shadowing from the grid. This relation is only true for device GA013. The variation of the fill factor (FF) is not pronounced and only device GA013 presents a FF higher than the others. Nonetheless these FF values are low compared to literature values for devices originating from co-evaporated and electrodeposited precursors [20,21]. Shafarman et al. obtained identical trends across the entire parameter range for co-evaporated devices with varying Ga content [12]. From the j–V curves it is possible to conclude that the efficiencies of the solar cells are hindered by the series resistance and the parallel conductance. The former parameter varies between 3.7 and 11.7 $\Omega \cdot cm^2$. As for the parallel conductance, it ranges from 1.0 to 12.4 $mS \cdot cm^{-2}$. However, these values are, on average, 50% lower than those extracted from the illuminated j–V curves, indicating there is an illumination dependent behaviour. Both the shunt conductance and the series resistance are ten times lower for solar cells with double the efficiency [12]. These factors help understand why the EQE response of the devices was mediocre. Additionally, the CIGS layer can also limit device performance, since PL results suggested that it is dominated by non-radiative recombination.

Fig. 1f shows the j–V curve for cell GA048, which had Cu/III = 0.98. A maximum 9.8% efficiency was obtained, with a V_{oc} of 676 mV and a J_{sc} of 27.1 $mA \cdot cm^{-2}$. Solar cells obtained from coevaporated absorbers with similar Ga/III ratio yielded V_{oc} = 801 mV and J_{sc} =28.5 $mA \cdot cm^{-2}$ [17]. The increase in the FF, relative to the previous series of solar cells, was the main factor behind the increase in efficiency. This is related to the decrease in the series resistance and in the shunt conductance. Still, there is a large difference between the parallel conductance in the dark and under illumination, showing that there is a light dependent behaviour. Additionally, both the series resistance and parallel conductance are still high when compared to literature values. A material property which can be responsible for these improvements is the Cu/III ratio of 0.98 of the absorber. In the previous set of solar cells, the highest efficiency was achieved for the absorber with the highest Cu/III ratio (GA013) as well and it is empirically known that the ideal value for the copper content is around 0.90 [13]. Thus, in the case of GA048, the higher copper content in combination with the higher gallium content delivered a device with efficiency higher than GA013. Fig. 1e presents the corresponding EQE of cell GA048. A maximum EQE of around 80% is observed and from integration a value of $J_{sc} = 30.7\ mA \cdot cm^{-2}$ was obtained. This value is more than 5% higher than the J_{sc} measured by IV, suggesting that, as previously observed, the absorber is not laterally homogenous. This result shows that further improvements are possible. At this time the source of the macroscopic lateral inhomogeneity is not understood.

4. Conclusion

In this work we have shown that the IEC 3-step reaction process is able to deliver CIGSSe absorbers without gallium segregation, originating from electrodeposited metal layers. The structural, optical and electrical properties of the absorbers and corresponding solar cells were studied as a function of the Ga/III. It was verified that all parameters varied according to both theoretical expectations and previous experimental studies. It was shown that the absorber consists of a CIGSe/CIGS system, with no signs of chalcogen intermixing. Additionally, it was observed that depending on the Ga content of the absorber, the optoelectronic properties changed due to a different Ga gradient at the of CIGSe/CIGS interface. The best solar cell showed an efficiency of 9.8% with a high V_{oc} of 676 mV. Nonetheless, these results were still hindered by high shunt conductance and series resistance. Moreover, no PL signal originating from the CIGS layer was observed, suggesting that this layer is defective and detrimental to device performance. To conclude, this work clearly demonstrates that the IEC 3-step reaction method is adequate and promising for EDA and that efficiencies above 10% can be achieved.

Acknowledgements

J.M., M.S. and P.D. thank the Fonds National de la Recherche du Luxembourg (1080203, CORE Junior Track Project C11/MS/1211521, and ATTRACT Fellowship Grant (07/06). J.S. acknowledges funding from the European project number FP7-PEOPLE-2012-ITN 316488. D.B. acknowledges Kevin Hart and John Elliot for their technical support. All authors would like to thank W.N. Shafarman for offering the use of the equipment at the Institute of Energy Conversion at the University of Delaware.

References

[1] D. Hermann, P. Kratzert, S. Weeke, M. Zimmer, J. Djordjevic-Reiss, R. Hunger, L. Bach, P. Lindberg, E. Wallin, O. Lundberg, L. Stolt, CIGS Module Manufacturing with High Deposition Rates and Efficiencies, 40th IEEE Photovoltaic Specialists Conference, Denver, Colorado, U.S.A., 2014.
[2] L. Ribeaucourt, E. Chassaing, G. Savidand, D. Lincot, Synthesis of Cu(In, Ga)Se-2 absorber using one-step electrodeposition of Cu–In–Ga precursor, Thin Solid Films 519 (2011) 7241.
[3] J.C. Malaquias, M. Steichen, M. Thomassey, P.J. Dale, Electrodeposition of Cu–In alloys from a choline chloride based deep eutectic solvent for photovoltaic applications, Electrochim. Acta 103 (2013) 15.
[4] J.C. Malaquias, D. Regesch, P.J. Dale, M. Steichen, Tuning the gallium content of metal precursors for Cu(In, Ga)Se-2 thin film solar cells by electrodeposition from a deep eutectic solvent, Phys. Chem. Chem. Phys. 16 (2014) 2561.
[5] M. Steichen, M. Thomassey, S. Siebentritt, P.J. Dale, Controlled electrodeposition of Cu–Ga from a deep eutectic solvent for low cost fabrication of $CuGaSe_2$ thin film solar cells, Phys. Chem. Chem. Phys. 13 (2011) 4292.
[6] J. Palm, V. Probst, W. Stetter, R. Toelle, S. Visbeck, H. Calwer, T. Niesen, H. Vogt, O. Hernandez, M. Wendl, F.H. Karg, CIGSSe thin film PV modules: from fundamental investigations to advanced performance and stability, Thin Solid Films 451 (2004) 544.

[7] W.K. Kim, G.M. Hanket, W.N. Shafarman, Ieee, Ga distribution and adhesion issues in selenization of metallic Cu–Ga–In precursors, 2009 34th IEEE Photovoltaic Specialists Conference, vols. 1–3, 2009, p. 2221.
[8] K. Kim, G.M. Hanket, H. Trang, W.N. Shafarman, Three-step $H_2Se/Ar/H_2S$ reaction of Cu–In–Ga precursors for controlled composition and adhesion of Cu(In, Ga)(Se, S)(2) thin films, J. Appl. Phys. 111 (2012).
[9] S.S. Hegedus, W.N. Shafarman, Thin-film solar cells: device measurements and analysis, Prog. Photovolt. Res. Appl. 12 (2004) 155.
[10] K. Yoshino, H. Yokoyama, K. Maeda, T. Ikari, Crystal growth and photoluminescence of $CuIn_XGa_{1-X}Se_2$ alloys, J. Cryst. Growth 211 (2000) 476.
[11] N.C. Halder, C.N.J. Wagner, Separation of particle size and lattice strain in integral breadth measurements, Acta Crystallogr. 20 (1966) 312.
[12] W.N. Shafarman, R. Klenk, B.E. McCandless, Device and material characterization of Cu(InGa)Se-2 solar cells with increasing band gap, J. Appl. Phys. 79 (1996) 7324.
[13] S.H. Han, F.S. Hasoon, J.W. Pankow, A.M. Hermann, D.H. Levi, Effect of Cu deficiency on the optical bowing of chalcopyrite $CuIn_{1-x}Ga_xSe_2$, Appl. Phys. Lett. 87 (2005).
[14] H.-T. Tung, I.-G. Chen, J.-M. Song, M.-G. Tsai, I.M. Kempson, G. Margaritondo, Y. Hwu, $Cu(In_{1-x}Ga_x)S$-2 nanocrystals and films: low-temperature synthesis with size and composition control, Nanoscale 5 (2013) 4706.
[15] M.I. Alonso, K. Wakita, J. Pascual, M. Garriga, N. Yamamoto, Optical functions and electronic structure of $CuInSe_2$, $CuGaSe_2$, $CuInS_2$, and $CuGaS_2$, Phys. Rev. B 63 (2001) 13.
[16] T. Dullweber, G. Hanna, W. Shams-Kolahi, A. Schwartzlander, M.A. Contreras, R. Noufi, H.W. Schock, Study of the effect of gallium grading in Cu(In, Ga)Se-2, Thin Solid Films 361 (2000) 478.
[17] M.A. Contreras, L.M. Mansfield, B. Egaas, J. Li, M. Romero, R. Noufi, E. Rudiger-Voigt, W. Mannstadt, Wide bandgap Cu(In, Ga)Se-2 solar cells with improved energy conversion efficiency, Prog. Photovolt. Res. Appl. 20 (2012) 843.
[18] M. Marudachalam, R.W. Birkmire, H. Hichri, J.M. Schultz, A. Swartzlander, M.M. AlJassim, Phases, morphology, and diffusion in $CuIn_xGa_{1-x}Se_2$ thin films, J. Appl. Phys. 82 (1997) 2896.
[19] S.M. Sze, Physics of Semiconductor Devices, Third ed. John Wiley & Sons Inc., New Jersey, United States of America, 2007.
[20] P. Jackson, D. Hariskos, E. Lotter, S. Paetel, R. Wuerz, R. Menner, W. Wischmann, M. Powalla, New world record efficiency for Cu(In, Ga)Se-2 thin-film solar cells beyond 20%, Prog. Photovolt. Res. Appl. 19 (2011) 894.
[21] R.N. Bhattacharya, CIGS-based solar cells prepared from electrodeposited stacked Cu/In/Ga layers, Sol. Energy Mater. Sol. Cells 113 (2013) 96.